PERIODICO di MINERALOGIA
established in 1930

DIPARTIMENTO
DI SCIENZE DELLA TERRA

SAPIENZA
UNIVERSITÀ DI ROMA

An International Journal of
Mineralogy, Crystallography, Geochemistry,
Ore Deposits, Petrology, Volcanology
and applied topics on Environment, Archaeometry and Cultural Heritage

Potential Alkali-Silica reactivity of Italian natural aggregates for concrete: assessment according to UNI 11530 and UNI 11604 standards

Gabriele Vola [1,*], Teresa Mangialardi [2], Umberto Costa [3]

[1] Geologist, building materials and industrial minerals specialist, via Finazzi 12h, Bergamo, Italy
[2] Department of Chemical Engineering Materials Environment, Sapienza University of Rome, Rome, Italy
[3] Chemist, cementitious materials, and technology specialist, Via Marzanica 15a, Bergamo, Italy

ARTICLE INFO

Submitted: February 2024
Accepted: June 2024
Available on line: June 2024

* Corresponding author:
gabriele.vola@gmail.com

Doi: 10.13133/2239-1002/18434

How to cite this article:
Vola G. et al. (2024)
Period. Mineral. 93, 105-125

ABSTRACT

The study focused on natural aggregates used in concrete, sourced from six different production sites in Italy, and assessed their potential alkali-silica reactivity through two national standard methods. The first method, UNI 11530, involved a detailed petrographic examination, utilizing modal analysis for identifying and quantifying potentially alkali-reactive lithotypes. The second test method, UNI 11604, involved an accelerated expansion test at 38 °C and high relative humidity on concrete including an established combination of size fractions of aggregates. This method allows the assessment of aggregate reactivity based on concrete expansion after 1 year of testing and an expansion limit value of 0.04%. A correlation analysis was done on the results from both test methods aimed to establish a relationship between the type and content of potentially reactive lithotypes of aggregates and concrete expansion. Chert and Chalcedony were identified as the primary contributors to concrete expansion. The sum of Chert and Chalcedony contents in the combined aggregates was found to vary between 1.8 vol% and 10.1 vol%. A critical content of approximately 5.5 vol% for the sum of Chert and Chalcedony was identified for deleterious expansion development in concrete subjected to UNI 11604 test method. This limit proves valuable in predicting the expansive behavior of aggregates where petrographic analysis has identified the presence of lithotypes potentially reactive to alkalis.

Keywords: Alkali-Silica reaction; Italian concrete and mortar aggregates; petrographic modal analysis, concrete prism expansion test; UNI 11530; UNI 11604.

INTRODUCTION

The alkali-silica reaction (ASR) that some aggregates can develop in the presence of alkalis (K_2O and Na_2O) is among the possible causes of concrete structures degradation. This reaction, whose course is often slow, can produce expansive effects of the concrete that put the integrity of the works at risk. The onset of the expansive reaction depends on the characteristics of the aggregates and the alkali content of the pore solution within the concrete, even if the environment in which the work is exposed, especially regarding humidity and temperature, can play an important role on the rate of the reaction and on the extent of degradation. The prevention of the alkali-silica reaction in new structures cannot disregard the evaluation of the potential alkali reactivity of the aggregate to be used in concrete and, consequently, may require the limitation of the alkali content of the concrete.

Wide research on these topics is available in the international literature (Sims and Poole, 2017), whose results have led to the development of guidelines for the

alkali-reactivity assessment of aggregates, such as the RILEM Recommendation AAR-0 (Rønning et al., 2021), and/or national standards applicable to local products.

In Italy the first identification of the phenomenon of the alkali-silica reaction occurred in 1982 following research into the causes of significant structural damage which occurred on industrial and hospital buildings built between 1972 and 1973 in an area on the Adriatic side of the Molise region (Levi et al., 1985). The subsequent extension of the investigations throughout the national territory highlighted other cases, documented in the literature, especially involving industrial flooring (Alunno Rossetti, 1981; Gasparotto et al., 2011) and some dams (Bon et al., 2001; Giuseppetti et al., 2003, Saouma and Perotti, 2005). Therefore, since the 80s of last century concrete aggregates have been the subject of extensive petrographic studies on thin sections, to ascertain the presence of phases potentially reactive to alkalis.

Aggregates which in the field have produced deleterious expansion phenomena are mostly from the alluvial deposits from the Apennine Mountains, composed of sedimentary rocks of Mesozoic and Cenozoic age: marls, limestones, shales, sandstones (all often siliceous with flint/chert, jasper and chalcedony in nodules and lenses) and clays. ASR phenomena have also been detected in other areas with volcanic formations (sometimes with jasper, opal, and chalcedony), granites and metamorphic rocks (i.e. gneisses, micaschists, granulites etc.) with deformed quartz (Barisone, 2001). More recently, Vola et al., 2011, developed a study involving 60 Italian aggregates, mainly from the Northern part of the country, especially from the Padana Valley. The reactivity of the aggregates was related to the presence of microcrystalline and cryptocrystalline quartz, generally defined as chert and/or flint, in sedimentary rocks, mostly carbonates, siliciclastic rocks, and alluvial deposits from the erosion of the Alpine and Apennine Mountain belts. Amorphous phase of volcanic rocks and strained quartz with undulatory extinction, mainly associated with metamorphic rocks, were considered potentially reactive too, although to a much lesser extent.

This research formed the basis according to which the current measures adopted in Italy to prevent ASR in new concrete primarily rely on the identification of potentially alkali-reactive lithologies by thin section petrography and point counting. However thin section petrography does not allow to reach conclusive diagnoses, particularly in the case of aggregates whose history of use is not known or in the case of very fine-grained rocks, such as siliceous limestones. Effectively, the optical identification of minerals becomes incrementally more difficult as the size of the grains decreases (Fernandes et al., 2014). For these reasons petrography is increasingly supported by complementary analytical techniques, especially X-ray powder diffraction (XRPD) analysis, scanning electron microscopy (SEM) coupled with energy dispersive spectroscopy (EDS), FT-IR, and TGA-DTA. These complementary investigations can be performed on aggregates as received (Fernandes et al., 2020; Medeiros et al., 2022), as well as on mortar bars after expansion tests to detect ASR gel formation (Marinoni et al., 2012; Custódio et al., 2022; Doğruyol, 2024).

Several deposits located in northern and central Italy have been investigated (Marinoni and Broekmans, 2013) using a promising new methodology based on the XRPD line profile analysis. The broadening of the X-ray diffraction of quartz peaks is modelled to extract microstructural parameters, i.e. crystallite size and microstrain, which reflect the presence of defect points, dislocations, twinning in the crystallographic lattice. Aggregate expansion behaviour has been assessed by the ultra-accelerated mortar bar test (UAMBT) according to RILEM AAR-2 to compare results. Therefore, line profile analysis by XRPD may be used to perform microstructural characterization of quartz, providing valuable information on its potential alkali reactivity towards ASR. Microstrain seems to be a more sensitive marker to ASR-reactivity of quartz than crystallite size showing, anyway, a large gap between the values of reactive and inert samples. Further research on the application of instrumental methods enabling a direct and rapid assessment of the alkali reactivity of the aggregates represents a current need to carry out an effective quality control mainly to detect intra-deposit variation.

However, for the time being the thin section petrography and the expansion testing on mortar or concrete are the methodologies envisaged by international recommendations and by the standards of various countries to assess the potential reactivity of the aggregates. These methods are still the subject of research aimed at refining the identification of the potentially reactive mineral phases using the petrographic method, implemented by digital image analysis for quantitative measurements (Antolik and Józwiak-Niedzwiedzka, 2021; Antolik et al., 2023) and in the case of expansion tests, to verify their reliability by comparing the expansive behaviour of concretes in laboratory and field tests (Borchers e al., 2022).

For the laboratory assessment of alkali-reactivity of aggregates, different mortar and/or concrete expansion test methods were investigated in Italy and some of them were considered as part of an experimental methodology proposed for evaluating the expansivity of aggregates, as well as of aggregate-cement combinations (Berra et al., 2015). Other than on pass-fail criteria, evaluation of the aggregate reactivity was based also on a parameter defined as Threshold Alkali Level (TAL), corresponding

to the concrete alkali content above which developed deleterious expansion. The suitability of such parameter as an index of the alkali reactivity of aggregates had already been assessed in previous research by comparing the results of different laboratory test methods on aggregates coming from 13 different Italian quarries. The proposed TAL-based reactivity classification resulted to be congruent with aggregates field behaviour (Berra et al., 2005). Research extended to combinations of aggregates with known TAL and blended cements containing hydraulically active mineral additions allowed to define a supplementary parameter, namely tolerable driving force (Δtol), useful for the selection of the blended cement to be used as a preventive measure against ASR for that specific concrete mix (Costa et al., 2014).

Further experimental research, specially designed with the purpose of refining the procedures of the above-mentioned test methods (Costa et al., 2017; Bavasso et al., 2020), was carried out at the Department of Chemical Materials Environment Engineering of Sapienza University of Rome, with the support of Unicemento. The results were the basis for the publication in the last decade of a package of standard test methods (i.e., UNI 11604, 2020; UNI 11504, 2021; and UNI 11530, 2023) concerning the assessment of the potential alkali-silica reactivity of aggregates. The criteria for evaluating the results of the above test methods and to assess the potential reactivity of aggregates are specified in (UNI 8520-22, 2020). Measures for preventing ASR in new concrete structures are recommended in (UNI 11417-2, 2022).

Another much rarer and not fully explained type of alkali-aggregate reaction, responsible for concrete distress, is the Alkali-Carbonate Reaction (ACR) caused by some types of argillaceous dolomite-bearing aggregates. Research, done on the aggregates susceptible to ACR, highlighted that generally, dolomite is accompanied by clay minerals and reactive silica minerals or phases, so that concrete expansion has been often related to ASR, particularly in case of aggregates containing fast-reactive silica forms such as chert, opal, and cryptocrystalline quartz (Jensen, 2012; Beyene et al., 2013; Beyene, 2018). As far as to the authors are aware, no case of concrete degradation due to ACR has been recognized in Italy, furthermore standard methods developed by UNI are not addressed to evaluating the potential alkali-carbonate reactivity of aggregates. Therefore, the present work, based on the application of standard test methods, was focused on ASR, also taking in consideration the mineralogical nature of the studied aggregates.

While considering that the current orientation of international research is aimed at evaluating the expansive behavior of cement-aggregate combinations to be used in the field by means of performance test methods such as RILEM AAR 10 (Rønning et al., 2021) and RILEM AAR 11 (Borchers et al., 2021), it should not be overlooked that the petrographic examination is an essential tool for evaluating the potential reactivity of aggregates for concrete or mortar and represents the starting point of the methodology of characterization of these materials.

This paper reports the qualitative and quantitative petrographic analysis, according to recently revised UNI 11530, on aggregates for concrete derived from different lithotypes widespread in Italy. The preliminary assessments of the alkali-silica reactivity, deduced from the presence of potential alkali-reactive constituents detected by petrographic analysis, and the results of point counting quantitative analysis of aggregates, were compared with accelerated expansion tests results on concrete according to UNI 11604. The purpose of the comparison was to find a relationship between the content and/or kind of potentially reactive constituents of the various aggregates and the expansive behavior of the relevant concretes subjected to standard test. An attempt was also made to identify a critical limit for the content of some potentially reactive constituents, as evaluated by the quantitative petrographic analysis (i.e, modal analysis on thin section).

MATERIALS AND METHODS

Aggregates classification

Six Italian aggregates for mortars and concrete were achieved thanks to different local producers and the Associazione Nazionale Estrattori Lapidei ed Affini (ANEPLA). Products, complying with the harmonized European standard UNI EN 12620, 2008), were supplied in the different grain size-fractions shown in Table 1 and Figure 1. The same table gives the type of aggregate, deduced from the grains morphology and a preliminary lithological (macroscopical) description, based on stereoscopic observation.

Petrographic analysis

The petrographic analysis was performed according to the recently revised Italian standard UNI 11530 dedicated to the detection and quantification of the potentially alkali-silica reactive lithotypes present in the aggregates for concrete. For this scope a polarizing light microscope (PLM) equipped with a high-resolution (4000x3000 pixel) digital camera was adopted. The quantitative analysis, i.e., volumetric modal analysis, was achieved by the point-counting method on a representative number of micrographs (i.e. 50-60 for each thin section) taken at 20x, under cross-polarized light (XPL). Two thin sections were prepared with grains 2-4 mm obtained by sieving the fine fractions of the aggregates (i.e. the sand) coming from

Table 1. Italian aggregates for mortar and concrete object of the research.

No.	Fraction's Code	Fraction's Denomination	Fraction's size	Aggregate Type	Preliminary Lithological description
1	1-A	Sand (B)	0-4 mm	Alluvial	Siliciclastic or terrigenous
	1-B	Gravel	8-15 mm		
	1-C	Gravel	15-22 mm		
2	2-A	Sand (B)	0-4 mm	Alluvial	Carbonatic
	2-B	Gravel	6-12 mm		
	2-C	Gravel	12-32 mm		
3	3-A	Crushed sand	0-4 mm	Crushed	Igneous Effusive (Volcanic)
	3-B	Crushed Rock	7-15 mm		
	3-C	Crushed Rock	10-18 mm		
4	4-A	Sand	0-4 mm	Alluvial	Metamorphic and Igneous intrusive
	4-B	Gravel	8-16 mm		
	4-C	Gravel	11-22 mm		
5	5-A	Sand	0-4 mm	Alluvial	Siliciclastic or terrigenous
	5-B	Gravel	4-8 mm		
	5-C	Gravel	4-14 mm		
	5-D	Gravel	11-22 mm		
6	6-A	Sand	0-4 mm	Alluvial	Siliciclastic and carbonatic
	6-B	Sand	0-8 mm		
	6-C	Gravel	8-14 mm		
	6-D	Gravel	11-22 mm		

each deposit. Furthermore, two additional thin sections with grains 2-4 mm were prepared by crushing and sieving the coarse fractions. Therefore, the total number of thin sections submitted to the modal analysis was 40. The description and recognition of the petrographic constituents were conducted in accordance with the current geological literature. Therefore, carbonate rocks were described according to the classifications proposed by (Dunham, 1962; Embry and Klovan, 1971; Sibley and Gregg, 1987; Tucker and Wright, 1990; Flügel, 2010). Moreover, the following terminology was adopted: 1) micrite refers to microcrystalline calcite crystals with size <4 μm; 2) microsparite indicates calcite crystals between 10-50 μm; and 3) sparite indicates clear calcite crystals larger than 62 μm. Terrigenous or siliciclastic rocks were described according to classic quartz, feldspar, and lithic fragments (QFL) triangular plot described by (Folk, 1980; Garzanti, 2019). The alizarine red staining method was adopted for distinguishing calcite from dolomite (Friedman, 1959). Igneous, and metamorphic rocks were described according to International Union of Geological Sciences (IUGS) recommendations (Streckeisen et al., 2002; Fettes and Desmons, 2007). Finally, the volcanic aggregate no. 3 was classified using TAS diagram according to Le Maitre (2005).

X-Ray Powder Diffraction analysis (XRPD)

XRPD analysis was adopted as a complementary analytical technique to evaluate the mineralogical composition of the aggregates, using aliquots taken from sub-samples finer than 1 mm (UNI 11530). A Rigaku Miniflex 600 diffractometer operating in a Bragg-Brentano geometry (1.5417 Å, 40 kV, and 40 mA), equipped with the D/teX Ultra-high-speed detector set to discriminate the Cu$Ka_{1,2}$ radiation, was adopted at this purpose. Samples were previously grinded in an agate mortar, then powders were back-loaded on an aluminum flat sample-holder and scanned in the angular range 5-90° of 2θ with a step size of 0.02° and a counting time of 0.4 s per step. Both identification and quantification of mineral phases were performed running the Rigaku PDXL2 software package. The Quantitative Phase Analysis (QPA) was carried out

Figure 1. Macroscopical picture of various grain-size fractions of aggregates investigated.

by the Whole Powder Pattern Fitting (WPPF) using the Rietveld method (Bish and Howard, 1988; Young, 1993). Crystallographic structures were selected on purpose from the literature.

Wavelength dispersive X-ray Fluorescence Spectroscopy (WD-XRF)

WD-XRF analysis was adopted as a complementary analytical technique to evaluate the chemical composition of the aggregates, using the same aliquots taken for the XRPD analysis. Samples were previously pulverized in a stainless-steel vessel ring mill. An aliquot of each sample was dried at 105 °C for a night and then burned at 1050 °C to determine the loss on ignition (LOI). Pressed pellets and fused beads methods were adopted for carbonate (aggregate no. 2) and silicate rocks (aggregates no. 1, 3, 4, 5, and 6), respectively. Powders were mixed with an organic binder wax (9:1 weight ratio) and then pelletized in 40 mm aluminum cups using a manual hydraulic press at 35 MPa for 1 min. Fusion beads were prepared by mixing 1 g of calcined powder with 10 g of lithium tetraborate/metaborate fusion flux (composition: 64.7 wt% Li tetraborate 35.3 wt% Li metaborate) using the Nieka

E1 fluxer for XRF Sample Preparation. The analysis was carried out using a Rigaku Supermini 200 wavelength dispersive X-ray fluorescence spectrometer (WD-XRF) with a Pd-anode operating at 200 W. Calibration curves were generated using available international standards of silicate and carbonate rocks. The calibration curves show a good linearity by pressed powder method for both major and minor components (Rigaku, 2015). Deviation values for repeatability tests are also very low.

Accelerated expansion test in concrete according to UNI 11604

The aggregates from each site were combined using their different size-fractions (Table 1) to fulfil the size gradation curve required by UNI 11604:2020 and prepare the test concrete. Figure 2 shows the grading requirements (dotted lines) and the grain size distribution curves of the combined test aggregates.

The combinations and the relevant fractions were characterized for their grain size distribution, dry density, and water absorption according to UNI EN 933-1:2012 and UNI EN 1097-6:2022. Table 2 gives the combinations composition, and the physical properties mentioned above of the combined aggregates and fractions.

A high alkali Portland cement CEM I 52.5 R conforming to UNI EN 197-1:2011 (1.05% as Na_2O_{eq} that is Na_2O_{eq}= Na_2O+0.658 K_2O; density of 3120 kg/m^3) was used in the concrete mixes. A total alkali content of the concrete equal to 5.5 kg Na_2O_{eq}/m^3 was obtained by adding appropriate amount of reagent-grade NaOH pellets to mixing water.

The concrete mix compositions, conforming to UNI 11604, are shown in Table 3. The relatively high cement content and the high alkali content of concrete are prescribed by the standard method to promote the reactivity of the aggregates.

A set of three prisms 75 mm x 75 mm x 285 mm in size was cast from each concrete mix. After 5 days precuring in a room at 20 °C ± 2°C and a relative humidity (RH) higher than 90% (1 day within the molds), the prisms were measured for their initial length (using a length comparator with a sensitivity of 0.001 mm) and weight, and then placed inside the storage containers recommended by UNI 11604. Stainless-steel containers, specially designed to limit alkali leaching from concrete prisms and tested in previous works (Costa et al., 2014, 2017) were cylindrical in shape (327 mm in inner height, and 135 mm in inner diameter), equipped with a perforated rack to store vertically one prism, and with an airtight closure. A 200-ml volume of deionized water was added to each container

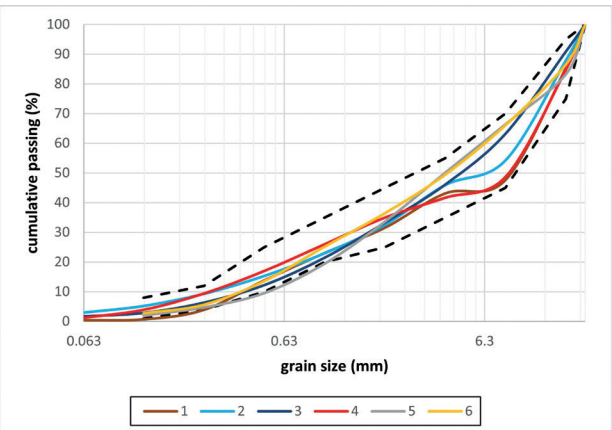

Figure 2. Grain size distribution curves of the combined test aggregates.

Table 2. Composition and physical properties of the combined test aggregates and the relevant fractions. Acronyms: ssd= saturated surface dry. Symbols: * values calculated based on proportion of the fractions in the concrete mix.

Aggregate and related raction No	Density of ssd granules	Water absorption	Fraction's proportion in concrete mix
Unit	[kg/m^3]	[Wt%]	[Wt%]
1	2584*	2.34*	
1-A	2593	2.30	45
1-B	2577	2.50	30
1-C	2578	2.20	25
2	2639*	1.30*	
2-A	2624	1.80	45
2-B	2647	1.00	30
2-C	2655	0.80	25
3	2635*	2.37*	
3-A	2604	3.20	45
3-B	2656	1.50	20
3-C	2662	1.80	35
4	2803*	0.83*	
4-A	2795	0.90	40
4-B	2795	0.90	35
4-C	2825	0.60	25
5	2607*	1.77*	
5-A	2600	1.60	50
5-B	2550	2.10	18
5-C	2650	1.90	12
5-D	2650	1.80	20
6	2666*	0.92*	
6-A	2660	0.80	8
6-B	2650	1.00	60
6-C	2690	0.90	4
6-D	2700	0.80	28

Table 3. Concrete mix compositions.

Concrete No.	Unit	1	2	3	4	5	6
Cement	(kg/m^3)	440	440	440	440	440	440
Deionized water	(kg/m^3)	220	220	220	220	220	220
NaOH pellets	(kg/m^3)	1.13	1.13	1.13	1.13	1.13	1.13
Combined aggregate	No.	1	2	3	4	5	6
	(kg/m^3)	1599.8	1633.6	1630.9	1734.7	1613.7	1649.3

before inserting the concrete specimen (water reserve), to create and maintain high relative humidity during the test (RH≥95%). The closed storage containers were put in a curing cabinet operating at 38 °C ± 2 °C. At established exposure times, up to an ultimate testing time of 400 days, and after cooling the closed containers for 16-18 h in a room kept at 20 °C ± 2° C, prism lengths and weights were measured. All measurements were performed on one specimen at a time, in a room with relative humidity not lower than 65% and were completed within 5 minutes to avoid concrete desiccation. The average percentage length change, ε_{av}%, was determined from each set of triplicate specimens at each exposure time. At the ultimate testing time specified by the test method (365 days), the values of sample standard deviation, s_c, (in case of $\varepsilon_{av\ 365}$%<0.02%) or coefficient of variation, CV%, (in case of $\varepsilon_{av\ 365}$%≥0.02%) were also evaluated for each set of measurements.

RESULTS

Chemical, mineralogical, and petrographic characterization of aggregates

Results of chemical (WD-XRF), and quantitative phase (XRPD-QPA) analyses of the aggregate combination, calculated from the proportions (see Table 2) of the grain size fractions in the concrete mix, are reported in Table 4 and Table 5, respectively. Moreover, results of petrographic quantitative analysis of each size fraction

Table 4. Chemical analysis of aggregates (WD-XRF). Lower Detection Limit = 0.01 wt%.
Acronym symbols: LOI = Loss on ignition; FB = Fused beads method; PP = Pressed pellets method.

Aggregate No.►		1	2	3	4	5	6
Determination▼	Unit	FB	PP	FB	FB	FB	FB
LOI	Wt%	18.33	41.27	3.66	1.34	9.77	12.63
SiO_2	Wt%	47.49	3.10	55.62	59.46	52.01	54.82
Al_2O_3	Wt%	5.78	0.32	17.93	15.84	5.08	9.78
Fe_2O_3	Wt%	2.95	0.41	7.48	7.31	6.26	2.90
CaO	Wt%	21.01	53.73	7.23	5.89	6.58	12.16
MgO	Wt%	1.03	0.73	3.29	3.37	18.18	3.58
SO_3	Wt%	0.29	0.06	0.07	0.07	0.02	0.02
Na_2O	Wt%	1.14	0.06	2.50	3.38	0.71	1.80
K_2O	Wt%	1.14	0.10	1.09	1.87	0.38	2.05
MnO	Wt%	0.23	0.07	0.20	0.08	0.14	0.04
SrO	Wt%	0.09	0.07	0.03	0.01	0.04	0.05
P_2O_5	Wt%	0.11	0.04	0.20	0.20	0.06	0.11
TiO_2	Wt%	0.23	0.02	0.70	1.08	0.35	0.30
Cr_2O_3	Wt%	<0.01	0.01	<0.01	<0.01	0.24	0.07
CuO	Wt%	0.01	0.01	<0.01	0.07	0.04	0.08
NiO	Wt%	<0.01	<0.01	<0.01	<0.01	0.10	<0.01
SUM	Wt%	99.80	100.00	100.00	100.00	100.00	100.40

Table 5. Quantitative Phase Analysis by the Rietveld method (XRPD-QPA) of aggregates.
Acronyms legend: Tr = traces (<0.1 wt%).

Aggregate No. ► Phase▼	Unit	1	2	3	4	5	6
Calcite	Wt%	38.7	95.3	1.6	0.3	7.1	11.6
Dolomite	Wt%	0.5	0.9	Tr	0.4	Tr	13.2
Quartz	Wt%	33.0	3.2	14.2	22.9	27.8	38.4
K-feldspar	Wt%	2.5			4.4	0.5	1.6
Plagioclase	Wt%	15.3	0.1	51.9	39.6	9.8	16.6
Muscovite/Illite	Wt%	4.9	0.5		11.3	4.8	14.1
Chlorite/Vermiculite	Wt%	4.6		14.5	4.5	4.5	2.2
Pyroxene	Wt%	0.4		2.3	0.4	3.6	
Amphibole	Wt%			3.6	6.6	3.0	1.2
Serpentine	Wt%			6.0	3.1	38.8	
Olivine	Wt%			2.9			
Epidote	Wt%				3.1	0.1	
Sillimanite	Wt%				Tr		
Laumontite	Wt%			1.0			
Cordierite	Wt%				2.4		
Titanite	Wt%				0.9	Tr	
Smectite	Wt%						1.2
Hematite/Goethite	Wt%			2.0	0.1		
SUM	Wt%	99.9	100.0	100.0	100.0	100.0	100.1

of the aggregate, namely volumetric modal analysis, are reported in Tables 6 a,b. Figures 3-8 shows representative micrographs of the most significant lithotypes of each aggregate. To enhance the readability of analytical data, the integrated chemical, mineralogical, and petrographic data of each aggregate are summarized below:

- Aggregate no. 1: Alluvial silicate-to-carbonate-bearing aggregate including siliciclastic or terrigenous lithotypes, and subordinately carbonate rocks too. The main elements are silicon (47.5 wt% as SiO_2) and calcium (21.0 wt% as CaO). Subordinated elements are aluminum (5.8 wt% as Al_2O_3), iron (3.0 wt% as Fe_2O_3), sodium (1.1 wt% as Na_2O), potassium (1.1 wt% as K_2O), and magnesium (1.0 wt% as MgO). Minor or trace elements are sulphur, titanium, manganese, phosphorus, and strontium. The mineral phases detected by XRPD-QPA are calcium carbonate (i.e., calcite, 38.7 wt%), quartz (33.0 wt%), and plagioclase (i.e., albite, 15.3 wt%). Subordinated phases are micaceous mineral (i.e., illite, 4.9 wt%), chlorite (i.e., clinochlore, 4.6 wt%), and K-feldspar (i.e. microcline, 2.5 wt%). The following accessory mineral phases were also detected: dolomite (0.5 wt%), and pyroxene (i.e., diopside, 0.4 wt%). These results are congruent with those of petrographic "modal" analysis because this aggregate is composed half of carbonate rocks (i.e., the content of carbonates ranges between 51.9 and 47.9 vol%), and the other half of silicate-bearing lithotypes, essentially terrigenous rocks (i.e., silicate-bearing rocks range between 35.8 and 45.8 vol%) (see Figure 3). Weathered rocks (max 4.7 vol% in sample 1-B), and opaque minerals (max 2.0 vol% in sample 1-A) are subordinated. Potentially alkali-silica reactive lithotypes are represented by micro and cryptocrystalline quartz (max 7.2 vol% in sample 1-A), chert (max 1.2 vol% in sample 1-B), and chalcedony (max 1.6 in sample 1-A).
- Aggregate no. 2: Alluvial carbonate-bearing aggregate is mainly composed of calcium (53.7 wt% as CaO). Very subordinated elements are silicon (3.1 wt% as SiO_2), magnesium (0.7 wt% as MgO), iron (0.4 wt% as Fe_2O_3), and aluminum (0.3 wt% as Al_2O_3). Trace elements are sulphur, sodium, potassium, manganese, strontium, and phosphorus. Loss of ignition is very high (41.3 wt%) due to prevailing presence of calcium carbonate (i.e. calcite, 95.3 wt%). Subordinated

Table 6a: Petrographic quantitative analysis, i.e. modal analysis, on aggregates no. 1, 2, and 3.
ASR potential lithotypes are highlighted with a grey background.
Acronyms legend: Pi = volumetric percentage; Pp %= proportionate volumetric percentage.

Aggregate No.►	Unit	1-A	1-B	1-C	1	2-A	2-B	2-C	2	3-A	3-B	3-C	3
Size ►	mm	0-4	8-15	15-22	.	0-4	6-12	12-32		0-4	7-15	10-18	
Lithotypes▼	Unit	Pi%	Pi%	Pi%	Pp %	Pi%	Pi%	Pi%	Pp %	Pi%	Pi%	Pi%	Pp %
Carbonate rocks (i.e., fossiliferous wackestones/packstones)	Vol%	49.7	51.9	47.9	49.9	23.1	26.5	22.6	24.0	-	-	-	-
Carbonate rocks (i.e., fossiliferous packstones/grainstones)	Vol%	-	-	-	-	61.3	66.3	69.1	64.7	-	-	-	-
Terrigenous rocks (i.e., sandstones and siltstones)	Vol%	29.8	24.3	26.2	27.3	-	-	-	-	-	-	-	-
Terrigenous rocks (i.e., calcarenites with detrital quartz grains)	Vol%	4.9	11.6	19.6	10.6	0.1	-	-	0.1	-	-	-	-
Terrigenous rocks (i.e., detrital quartz grains)	Vol%	-	-	-	-	-	-	-	-	-	-	-	-
Igneous intrusive rocks (i.e. granites)	Vol%	1.1	-	-	0.5	-	-	-	-	-	-	-	-
Calcite phenocrysts in effusive rocks (i.e. andesite)	Vol%									1.3	1.2	2.3	1.6
Andesine phenocrysts in effusive rocks (i.e. andesite)	Vol%	-	-	-	-	-	-	-	-	44.1	54.0	42.1	45.4
Quartz phenocrysts in effusive rocks (i.e. andesite)	Vol%	-	-	-	-	-	-	-	-	0.2	1.2	0.1	0.4
Hornblende phenocrysts in effusive rocks (i.e. andesite)	Vol%	-	-	-	-	-	-	-	-	5.1	8.5	15.1	9.2
Augite/biotite phenocrysts in effusive rocks (i.e. andesite)	Vol%	-	-	-	-	-	-	-	-	0.7	0.4	-	0.4
Alteration chlorite in effusive rocks (i.e. andesite)	Vol%	-	-	-	-	-	-	-	-	17.3	16.9	22.1	18.9
Alteration zeolite in effusive rocks (i.e. andesite)	Vol%	-	-	-	-	-	-	-	-	1.2	0.2	0.6	0.8
Weathered rocks (including serpentinites, and limonite)	Vol%	2.8	4.7	1.7	3.1	1.3	-	-	0.6	-	-	-	-
Opaque minerals	Vol%	2.0	1.4	0.5	1.4	0.3	1.0	-	0.4	4.0	5.2	4.9	4.5
Chalcedony in sedimentary rocks	Vol%	1.6	1.1	-	1.0	1.9	0.6	1.6	1.4	-	-	-	-
Chert in sedimentary rocks	Vol%	0.9	1.2	-	0.8	12.0	5.6	6.6	8.7	-	-	-	-
Microcrystalline quartz in terrigenous rocks	Vol%	7.2	3.8	4.0	5.4	-	-	-	-	-	-	-	-
Groundmass in effusive rocks (i.e. andesite)	Vol%	-	-	-	-	-	-	-	-	26.1	12.5	12.9	18.9
SUM	Vol%	100.0	100.1	99.9	100.1	100.1	100.0	99.9	99.9	100.0	100.1	100.1	100.1
Points	no.	3933	4859	4028	-	4336	4364	4318	-	4894	4952	4976	-

Table 6b. Petrographic quantitative analysis, i.e. volumetric modal analysis on aggregates no. 4, 5, and 6.
ASR potential lithotypes are highlighted with a grey background.
Acronyms legend: Pi (%) = volumetric percentage; Pp %= proportionate volumetric percentage.

Aggregate No.►	Unit	4-A	4-B	4-C	4	5-A	5-B	5-C	5-D	5	6-A	6-B	6-C	6-D	6
Size ►	mm	0-4	8-15	15-22		0-4	4-8	4-14	11-22		0-4	0-8	8-14	11-22	
Lithotypes▼	Unit	Pi (%)	Pi (%)	Pi (%)	Pp %	Pi (%)	Pi (%)	Pi (%)	Pi (%)	Pp %	Pi (%)	Pi (%)	Pi (%)	Pi (%)	Pp %
Carbonate rocks (i.e. microsparite, sparite and calcitic veins)	Vol%	-	-	-	-	6.0	4.3	7.1	9.8	6.6	18.0	19.4	31.5	28.7	22.4
Carbonate rocks (i.e., dolostones)	Vol%	-	-	-	-	-	-	-	-	-	9.3	5.7	10.6	6.5	6.4
Terrigenous rocks (i.e., calcarenites)	Vol%	-	-	-	-	2.9	0.8	7.6	18.5	6.2	-	-	-	-	-
Terrigenous rocks (i.e. sandstones and siltstones)	Vol%	-	-	-	-	-	-	-	-	-	0.7	1.4	0.9	-	0.9
Igneous intrusive (Intermediate) and metamorphic rocks (i.e. diorites and dioritic gneisses)	Vol%	42.8	34.0	46.0	40.5	-	-	-	-	-	-	-	-	-	-
Igneous intrusive (acid) and metamorphic rocks (i.e. granites, granodiorites, gneisses, and micaschists)	Vol%	38.7	35.5	34.3	36.5	-	-	-	-	-	32.3	21.4	20.2	24.4	23.0
Igneous intrusive (mafic) and metamorphic rocks (i.e., prasinites and amphibolites)	Vol%	-	-	-	-	-	-	-	-	-	2.6	2.3	2.8	-	1.7
Igneous intrusive (acid) rocks (i.e. mono-polycrystalline quartz fragments)	Vol%	-	-	-	-	9.4	12.5	3.5	2.2	7.8	8.6	11.3	3.9	2.7	8.3
Igneous intrusive rocks (i.e. mafic rocks) and alteration products	Vol%	12.9	22.8	14.4	16.7	-	-	-	-	-	-	-	-	-	-
Igneous effusive rocks (i.e. different types)	Vol%	-	-	-	-	3.2	-	4.1	2.3	2.5	7.4	12.6	5.6	5.1	9.8
Metamorphic rocks (i.e., serpentinites)	Vol%	2.0	0.9	2.8	1.8	34.7	49.6	40.0	45.4	40.2	-	-	-	-	-
Metamorphic rocks (i.e., amphibolites and micaschists)	Vol%	-	-	-	-	16.0	10.1	12.1	4.0	12.1	-	-	-	-	-
Weathered rocks (i.e., limonite and sericite)	Vol%	-	-	-	-	4.4	8.1	2.0	6.9	5.3	-	-	-	-	-
Opaque minerals	Vol%	0.6	1.4	1.9	1.2	4.8	3.1	4.5	2.9	4.1	1.0	0.3	1.2	0.9	0.5
Siliceous matrix in terrigenous rocks	Vol%	-	-	-	-	7.0	5.8	12.9	5.0	7.1	-	-	-	-	-
Chalcedony in sedimentary rocks	Vol%	-	-	-	-	-	-	-	-	-	1.6	2.2	1.4	2.0	2.1
Chert in sedimentary rocks	Vol%	-	-	-	-	3.4	1.6	4.8	2.0	2.9	3.7	5.5	4.0	4.6	5.0
Micro and cryptocrystalline quartz	Vol%	2.9	5.4	0.6	3.2	7.3	4.1	0.5	0.7	4.6	6.6	6.1	6.1	3.9	5.5
Groundmass of effusive rocks	Vol%	-	-	-	-	1.0	-	0.8	0.4	0.7	8.2	11.9	11.8	21.2	14.2
SUM	Vol%	99.9	100.0	100.0	99.9	100.1	100.0	99.9	100.1	100.1	100.0	100.1	100.0	100.0	99.8
Points	no.	4119	3753	4407	-	3868	4518	5160	4348	-	3751	3622	4152	5041	-

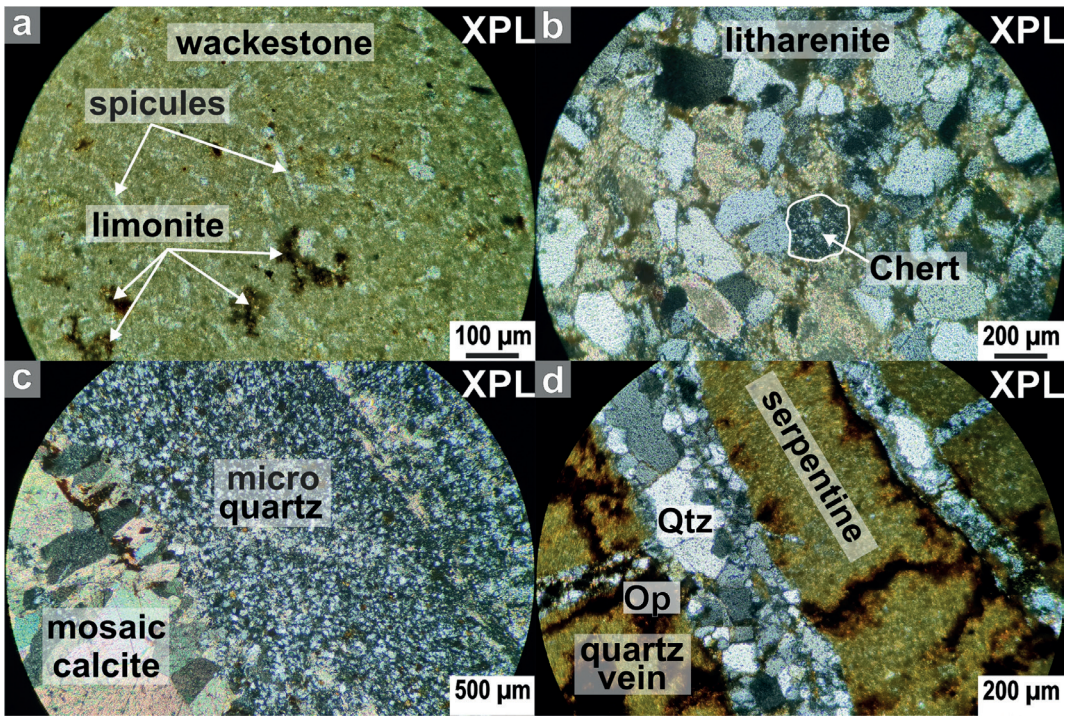

Figure 3. Petrographic analysis of aggregate sample no. 1. Alluvial silicate-to-carbonate bearing aggregate. Micrographs details: a) fossiliferous wackestone with echinoid spicules and limonite plagues, b) carbonate-cemented litharenite composed of various detrital grains, including quartz, calcite, feldspars, muscovite, chlorite, chert, and opaque minerals, c) microcrystalline quartz associate with mosaic calcite and dogtooth spar; d) weathered rock (i.e. probably altered serpentine rock) cut by a quartz vein, displaying macro-to-microcrystalline quartz (Qtz), and opaque minerals (Op).

mineral phases are quartz (3.2 wt%), and dolomite (0.9 wt%). The following accessory mineral phases were also detected: a micaceous mineral (i.e., illite, 0.5 wt%) and plagioclase (i.e. albite, 0.1 wt%). The fundamental lithological types are represented by various carbonate rocks, including fossiliferous packstone-grainstones (max 69.1 vol% in sample 2-C), and fossiliferous mudstone-wackestones (max 26.5 vol% in sample 2-B) (see Figure 4). Weathered rocks, opaque minerals, and detrital quartz grains are present in minor amount. Potentially alkali-silica reactive lithotypes are represented by chert (max 12.0 vol% in sample 2-A), and chalcedony (max 1.9 vol% in sample 2-A).

- Aggregate no. 3: Crushed silicate-bearing volcanic aggregate that plots in the field of basaltic andesite according to TAS diagram for volcanic rocks. Silicon as SiO_2 and aluminum as Al_2O_3 contents are 55.6 wt% and 17.9% wt%, respectively. Subordinated elements are iron (7.5 wt% as Fe_2O_3), calcium (7.2 wt% as CaO) and magnesium (3.3 wt% as MgO) and alkalis (2.5 wt% of Na_2O, and 1.1 wt% of K_2O). Minor or trace elements are titanium, manganese, phosphorus, and strontium. The main mineral phases are plagioclase (i.e., andesine, 51.9 wt%), quartz (14.2 wt%) and chlorites (i.e. clinochlore/vermiculite,14.5 wt%). Subordinated minerals phases are pyroxenes, amphiboles, serpentines, olivine, and iron oxides (i.e., hematite). Alteration phases are calcite, laumontite, and iron hydroxides (i.e. goethite). From the petrographic perspective this aggregate is essentially composed of volcanic or subvolcanic (i.e. hypabyssal) andesite rock, exhibiting a typical porphyritic texture with various phenocrysts dispersed within a fine-grained and/or glassy groundmass (see Figure 5). Fundamental primary phenocrysts are plagioclase (i.e., andesine, max 54.0 vol % in sample 3-B), green hornblende (max 15.1 vol% in sample 3-C), quartz (max 1.2 vol% in sample 3-B), pyroxene (i.e. augite), and biotite in small amount. Secondary mineral phases, i.e. alteration products, are mainly constituted of chlorite (max 22.1 vol% in sample 3-C), calcite (max 2.3 vol% in sample 3-C), and zeolite (max 1.2 in sample 3-A). Potentially alkali-silica reactive lithotype is represented by the fine-grained to vitreous or glassy groundmass ranging between 26.1 and 12.5 vol%.
- Aggregate no. 4: Alluvial silicate-bearing aggregate

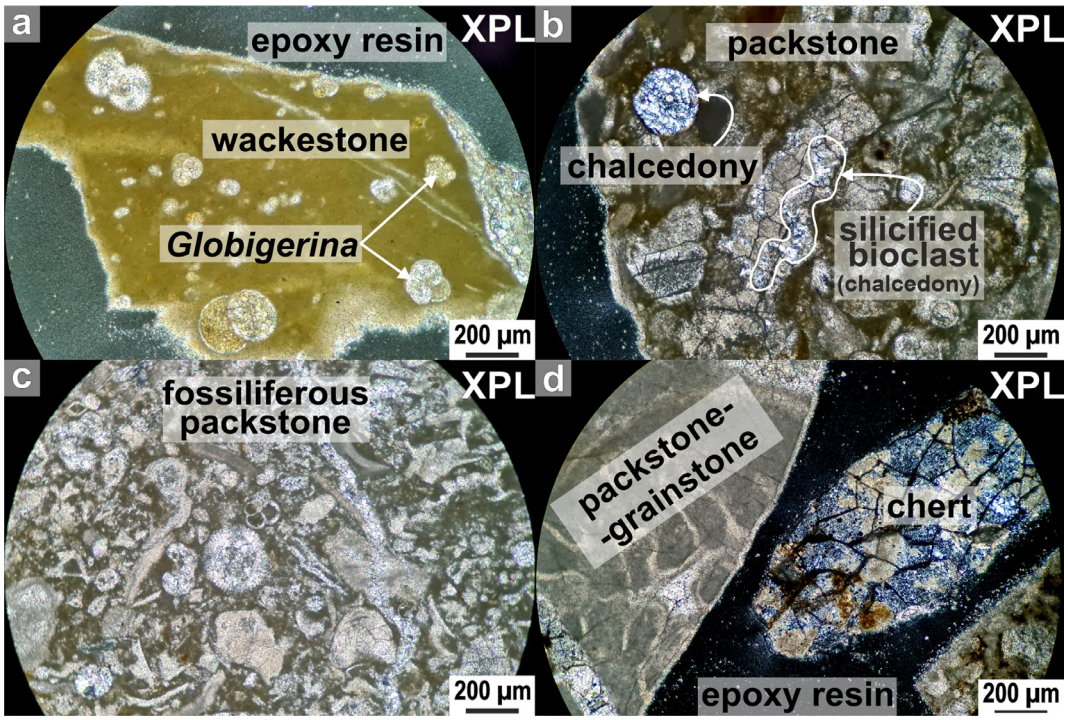

Figure 4. Petrographic analysis of aggregate sample no. 2. Alluvial carbonate aggregate. Micrographs details: a) fossiliferous wackestone constituted of micrite and planktonic foraminifera (Globigerina), b) poorly sorted packstone with planktonic foraminifera, bivalves, gastropods, echinoderms, sporadic silicified bioclasts and chalcedonic spherules. These last lithotype is potentially alkali-silica reactive, c-d); fossiliferous packstone-to-grainstone containing agglutinated benthonic foraminifera, red algae, echinoids, and secondary veins with mosaic calcite, and chert grains. This last constituent is potentially alkali-silica reactive lithotype. Legend symbols: XPL = cross-polarized light.

essentially composed of various silicate rocks. Main elements are silicon (59.5 wt% as SiO_2), aluminum (15.8 wt% as Al_2O_3), and iron (7.3 wt% as Fe_2O_3). Subordinated elements are calcium (5.9 wt% as CaO), magnesium (3.4 wt% as MgO), and alkalis (3.4 wt% of Na_2O, and 1.9 wt% of K_2O). Minor or trace elements are titanium, phosphorus, manganese, sulphur, and copper. The main mineral phases are plagioclase (i.e., oligoclase, 39.6 wt%), quartz (22.9 wt%), a micaceous mineral (i.e. muscovite, 11.3 wt%), and amphiboles (i.e., riebeckite/ferrotschermakite 6.6 wt%). Subordinated mineral phases are chlorite (i.e., clinochlore/vermiculite 4.5 wt%), K-feldspar (i.e., microcline 4.4 wt%), serpentine (i.e., antigorite/lizardite 3.1 wt%), epidote (i.e., clinozoisite 3.1 wt%), and cordierite (2.4 wt%). Accessory minerals are pyroxene (i.e., augite), sillimanite, and titanite. Chemical and mineralogical analyses align with the findings from the petrographic examination. The volumetric modal analysis effectively highlights the substantial presence of various silicate-bearing intrusive and metamorphic rocks (see Figure 6). Specifically, acid-to-intermediate rocks, such as granites, granodiorites, diorites, and related gneisses, and micaschists range between 69.5 and 81.5 vol%. Additionally, mafic intrusive rocks vary between 12.9 and 22.8 vol%. Other lithotypes, including serpentinites and opaque minerals, are subordinated. Furthermore, potentially alkali-silica reactive lithotypes are primarily composed of micro and cryptocrystalline quartz, ranging between 0.6 to 5.4 vol%.

- Aggregate no. 5: Alluvial silicate-bearing aggregate is primary composed of various silicate rocks, with carbonate rocks playing a subordinate role. Main elements are silicon (52.0 wt% as SiO_2), magnesium (18.2 wt% as MgO), calcium (6.6 wt% as CaO), iron (6.3 Wt% as Fe_2O_3), aluminum (5.1 wt% as Al_2O_3). Subordinated elements are alkalis (0.7 wt% of Na_2O, and 0.4 wt% of K_2O), and titanium (0.4 wt% as TiO_2). Minor or trace elements are chromium, manganese, and phosphorus. The main mineral phases detected by XRPD-QPA are serpentine (i.e., antigorite/lizardite, 38.8 wt%), quartz (27.8 wt%), and plagioclase (i.e. albite, 9.8 wt%). Subordinated mineral phases are calcium carbonate (i.e., calcite 7.1 wt%), a micaceous

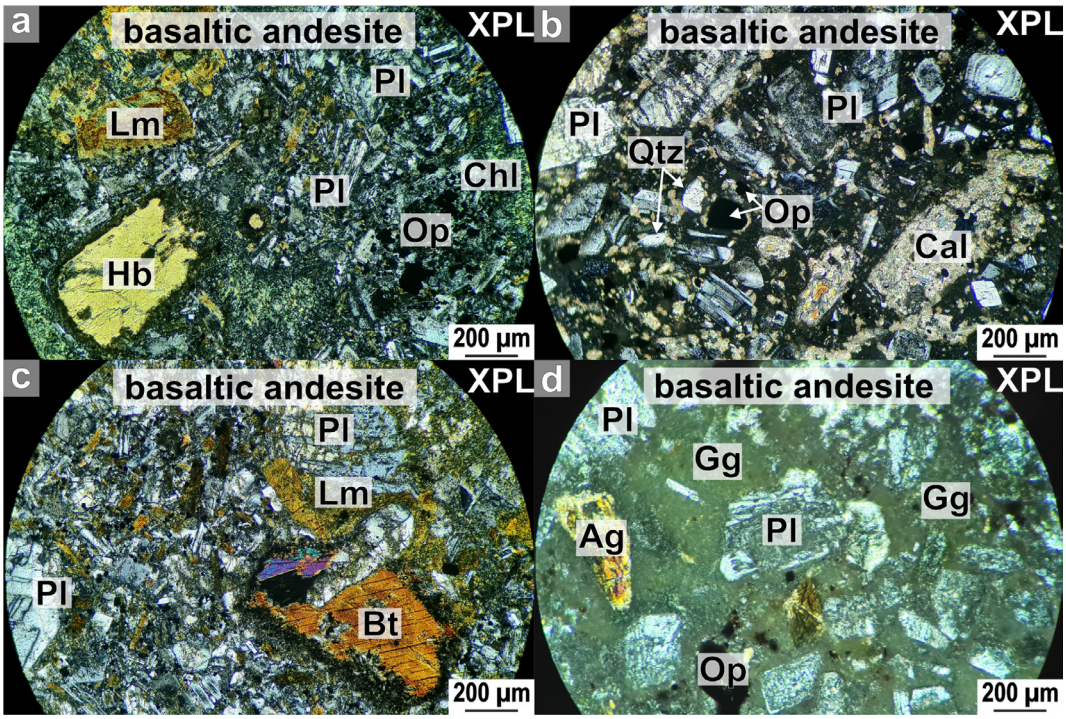

Figure 5. Petrographic analysis of aggregate sample no. 3. Crushed volcanic-to-subvolcanic basaltic andesite aggregate exhibiting typical porphyritic texture. Various magmatic phenocrysts are dispersed within the fine-grained matrix, which is composed of micro-to-cryptocrystalline and/or glassy groundmass (Gg). This last lithotype is considered potentially alkali-silica reactive. The following primary (i.e. magmatic) phenocrysts can be also observed: zoned crystals of plagioclase (Pl) with prismatic habitus and spongy or skeletal texture; interstitial fine-grained quartz (Qtz); green hornblende (Hb); pyroxene, i.e. augite (Ag), and biotite (Bt). Secondary (i.e. alteration) phenocrysts are constituted of chlorite (Chl), sericite, limonite (Lm), calcite (Cal) and zeolite, and opaque minerals (Op).

mineral (i.e., muscovite/illite 4.8 wt%), chlorite (i.e., clinochlore/vermiculite 4.5 wt%), pyroxene (i.e., ferrosilite/hedenbergite 3.6 wt%), and amphibole (i.e., actinolite/glaucophane 3.0 wt%). Accessory minerals are K-feldspar and epidote, dolomite, and titanite. From the petrographic perspective, this aggregate is essentially composed of silicate-bearing metamorphic rocks, namely serpentinites, and to a lesser extent, magmatic intrusive, and effusive rocks (see Figure 7). Additionally, it includes amphibolites, micaschists, terrigenous, and carbonate rocks. Specifically, serpentinites account for 34.7 and 49.6 vol%, intrusive acid-to-intermediate rocks between 2.2 and 9.4 vol%, mafic effusive rocks make up 2.3 and 4.1 vol%, and other metamorphic rocks contribute 4.0 and 16.0 vol%. Terrigenous and carbonate rocks play a subordinate role, with volumes contents varying between 0.8 and 18.5 vol% and 4.3 and 9.8 vol%, respectively. Weathered rocks ranges between 2.0 and 8.1 vol%, while opaque minerals contribute 2.9 and 4.8 vol%. Finally, potentially alkali-silica reactive lithotypes include the siliceous matrix in terrigenous rocks (max 12.9 vol% in sample 5-C), micro and cryptocrystalline quartz (7.3 vol% in sample 5-A), chert (4.8 vol% in sample 5-C), and groundmass of effusive rocks (1.0 vol% in sample 5-A).

- Aggregate no. 6: Alluvial silicate-bearing aggregate is mainly composed of silicate rocks, and subordinately of carbonate rocks too. Main elements are silicon (54.8 wt% as SiO_2), calcium (12.2 wt%, as CaO), and aluminum (9.8 wt% as Al_2O_3). Subordinated elements are magnesium (3.6 wt% as MgO), iron (2.9 wt% as Fe_2O_3), and alkalis (1.8 wt% of Na_2O, and 2.1 wt% of K_2O). Minor or trace elements are titanium, phosphorus, chromium, copper, strontium, and manganese. The main mineral phases are quartz (38.4 wt%), plagioclase (i.e., oligoclase, 16.6 wt%), a micaceous mineral (i.e. muscovite/illite 14.1 wt%), dolomite (13.2 wt%), and calcite (11.6 wt%). Subordinated mineral phases are K-feldspar (i.e., microcline 1.6 wt%), and amphibole (i.e., hornblende 1.2 wt%). Alteration phases are constituted by clay minerals (i.e., smectite 1.2 wt%). The petrographic examination, specifically volumetric modal

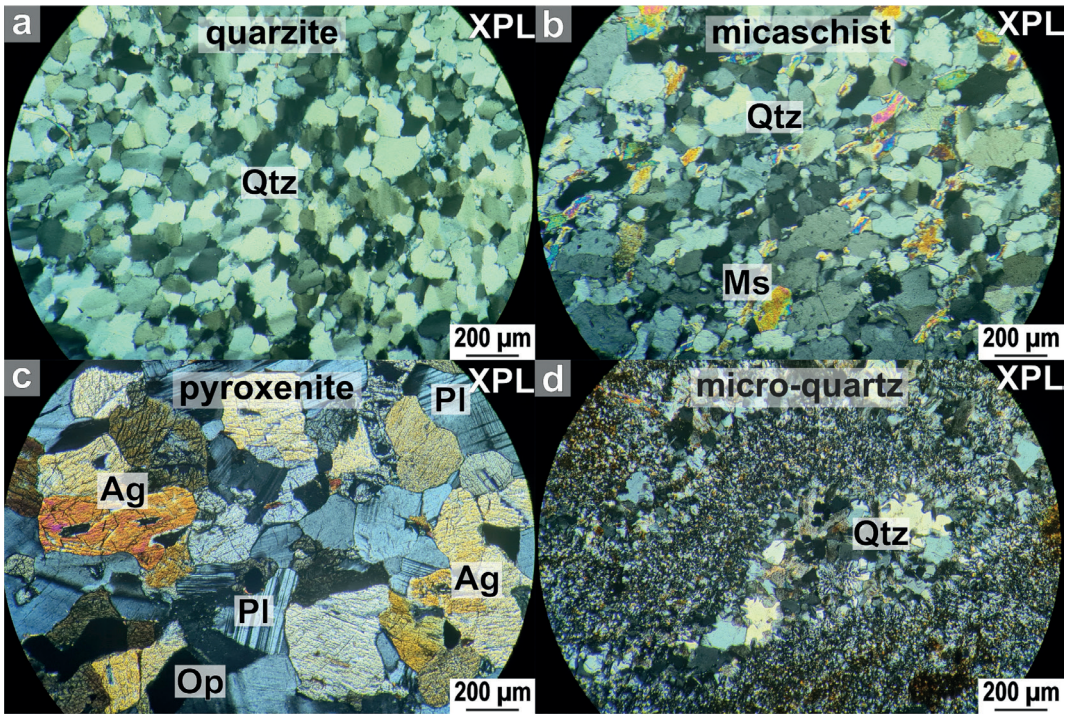

Figure 6. Petrographic analysis of aggregate sample no. 4. Alluvial silicate-bearing aggregate, including igneous intrusive, effusive, and metamorphic rocks. Micrographs details: a) weakly schistose quartzite, composed of homogeneous texture of 10-50 microns quartz (Qtz) porphyroblasts, b) moderately schistose micaschist composed of quartz, K-feldspar, plagioclase, and muscovite, c) igneous intrusive mafic rock, i.e. pyroxenite, composed of augite (Ag), and plagioclase (Pl), d) potentially alkali-silica reactive microcrystalline quartz associated with large, i.e. 50-100 microns, quartz (Qtz) porphyroblasts. Legend symbols: XPL = cross-polarized light.

analysis, highlights the following key lithotypes: silicate-bearing intrusive, effusive, or volcanic, metamorphic, as well as siliciclastic or terrigenous, and carbonate rocks (see Figure 8). All the silicate-bearing rocks mentioned earlier, taken as a whole, fall within the range of 51.6 to 32.2 vol%. Various carbonates, including microsparite, sparite, calcitic veins, and dolostones vary between 25.1 and 42.1 vol%. Opaque minerals are present up to 1.2 vol% in sample 6-C. Additionally, the following potentially alkali-silica reactive lithotypes were detected, including the groundmass of effusive rocks (from 8.2 to 21.2 vol%), micro and cryptocrystalline quartz (from 3.9 to 6.6 vol%), chert (from 3.7 to 5.5 vol%), and chalcedony (from 1.4 to 2.2 vol%). Furthermore, a significant content of dolomite rocks, susceptible of alkali-carbonate reaction, have been detected, as well. They vary between 5.7 and 10.6 vol%. It is worth nothing to note that predominant lithofacies is constituted by a hypidiotopic mosaic of medium-to-coarse grained dolomite crystals, according to the classification of Sibley and Gregg (1987). However, this last lithofacies does not fall among those indicated by Tritsch (2018) as having potential for expansive alkali-carbonate reaction.

Expansion test of concrete prisms

Figure 9 shows the trends of the average percentage changes in length of concrete prisms (expansions, ε_{av}%), calculated for the various concrete mixes, as a function of testing time. In this figure, a dashed line representing the expansion limit at 365 days of testing (0.04%) is also drawn. According to Italian standard UNI 8520-22 (2020), concrete expansion above this limit (deleterious expansion) indicates the potential reactivity of the tested aggregate. Statistical evaluation of the results obtained after 365 days of testing revealed the acceptability of all the measurements (see Table 7).

For all groups of samples, exception made for those containing aggregates from source 5, the standard deviation, s_c, in case of $\varepsilon_{365\ av}$%<0.02%, or the coefficient of variation, in case of $\varepsilon_{365\ av}$%≥0.02%, were lower than the respective values established for the repeatability of the test method (σ=0.0025% and CV=12%). However, for the aggregate no. 5, the dispersion of the experimental results still satisfied the acceptability criterion specified

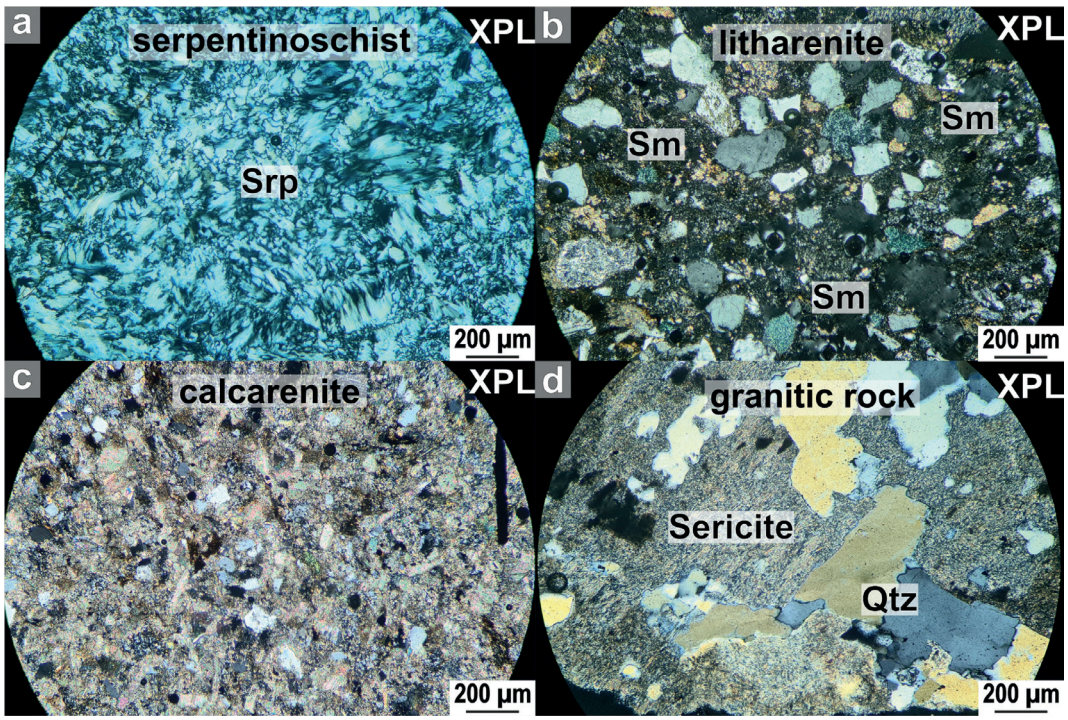

Figure 7. Petrographic analysis of aggregate sample no. 5. Alluvial silicate-bearing aggregate, including igneous intrusive, effusive, metamorphic, and terrigenous rocks. Micrographs details: a) serpentinoschist rock is mostly composed of minerals from the serpentine group (Srp). It typically exhibits a scaly or lamellar texture, occasionally transitioning to a microcrystalline texture, b) litharenite is composed of different detrital grains including quartz, altered feldspars, serpentine, and sparite. In this case, the cementing matrix is siliceous (Sm), c) calcarenite is composed of fine-grained detrital grains including bioclasts, sparite, quartz, and occasionally chert. In this case, the cementing matrix is micritic, d) weathered granitic rock essentially composed of quartz grains and altered feldspars, presenting microcrystalline texture with fine-grained micaceous minerals (i.e. sericite). Legend symbols: XPL = cross-polarized light.

by UNI 11604 for a confidence level of 95%. In particular, the ratio between the sample standard deviation, s_c, and the standard deviation of the test method, σ, fell within the acceptable range specified for a number of data equal to three [see equation (1)]:

$$0.159<s_c/\sigma<1.920 \quad (1)$$

In eq. (1), the values of σ are dependent on the expansions at 365 days, and were obtained as follows:

$\sigma=0.0025$ for $\varepsilon_{365\ av}\%<0.02\%$
$\sigma=0.12\ \varepsilon_{365\ av}\%$ for $\varepsilon_{365\ av}\%\ 0.02\%$

Based on the expansions at 365 days and the reactivity criterion shown in Figure 9, only aggregates no. 2 and 6 may be considered alkali-silica reactive in concrete, with $\varepsilon_{365\ av}\%$ values of 0.078% and 0.051%, respectively. Considering the trend of the curves, aggregate no. 2 reveals to be more expansive than aggregate no. 6 over the whole testing time, and its expansivity is more rapidly developed. After about 200 days of testing, concrete with aggregate no. 2 develops about 86% of the expansion at the ultimate testing time, while concrete with aggregate no. 6 reaches only about 49% of the ultimate expansion. However, neither curve levels up at 365 days, so indicating that the expansion potential of the two aggregates is not exhausted under the testing conditions.

Irrespective of their expansion level, concrete prisms underwent similar weight increases during the 400 days of testing, ranging from 20 to 25 g. This confirmed the suitability of testing conditions to maintain high relative humidity allowing the cement hydration and, in some cases, the alkali-silica reaction.

Visual inspection of concrete prisms revealed the presence of white and brownish efflorescence on the surface of most concrete prisms, regardless of their expansion, so indicating the presence of leaching and/or exudation phenomena involving alkalis and/or ASR products (Jensen, 2020). After about six months of testing, thin and irregular cracks were visible on the surface of concrete prisms containing aggregate no. 2.

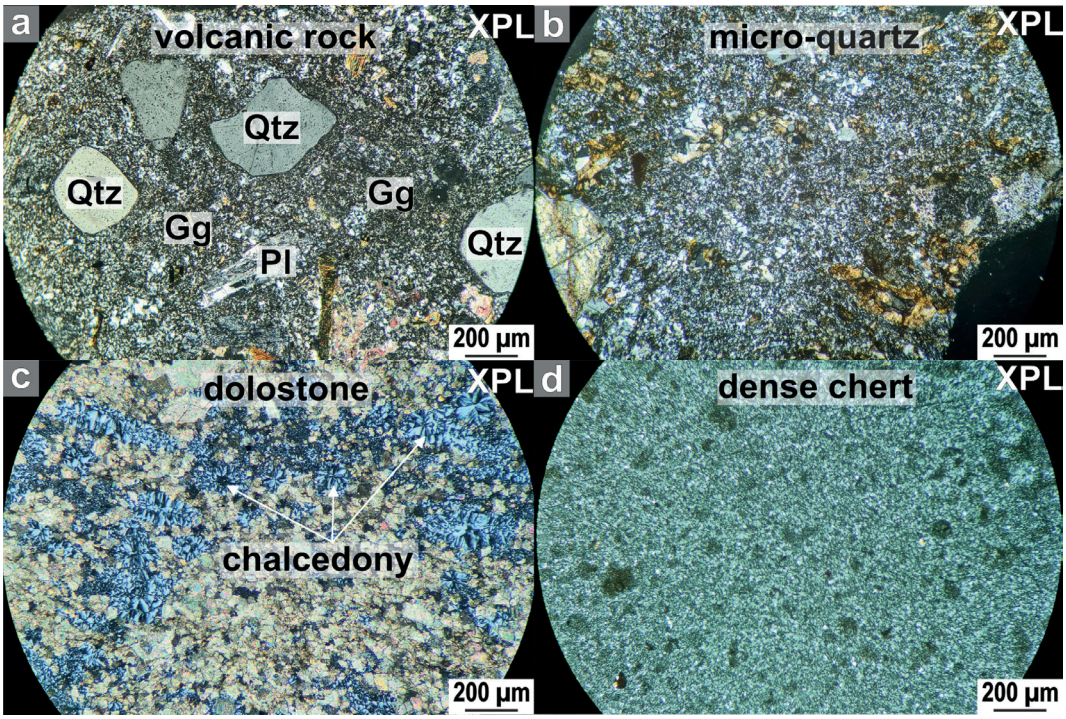

Figure 8. Petrographic analysis of aggregate sample no. 6. Alluvial silicate-bearing aggregate, including igneous intrusive, effusive, metamorphic, and, subordinately, carbonate and terrigenous rocks. Micrographs details: a) volcanic rock exhibiting typical porphyritic texture with primary phenocrysts composed of rounded quartz (Qtz) and altered spongy or skeletal plagioclases (Pl). The fine-grained matrix occasionally transitions to a glassy groundmass (Gg), b) terrigenous rock presenting potentially alkali-silica reactive microcrystalline quartz, c) dolostone presenting large portions of the rock substituted by fibrous chalcedony. This last lithotype is potentially alkali-silica reactive, d) large grain of dense chert exhibiting remnants of its primary sedimentary texture. This last lithotype is potentially alkali-silica reactive too. Legend symbols: XPL = cross-polarized light.

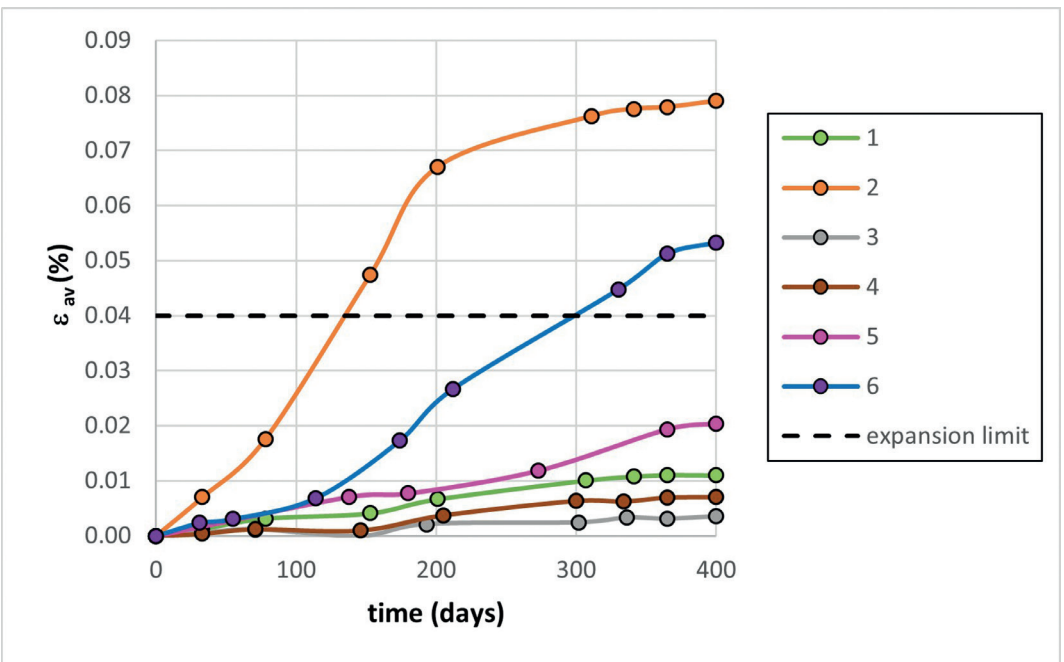

Figure 9. Expansion curves of concrete prisms subjected to standard test UNI 11604.

Table 7. Statistical evaluation of concrete expansion test results. Unsatisfactory results are in bold.

Concrete	$\varepsilon_{365\ av}$ (%)	s_c	CV (%)	σ	s_c/σ
1	0.011	0.0012		0.0025	0.480
2	0.078	0.0018	2.26	0.0093	0.188
3	0.003	0.0017		0.0025	0.696
4	0.007	0.0012		0.0025	0.487
5	0.019	0.0048		0.0025	1.909
6	0.051	0.0027	6.24	0.0053	0.520

DISCUSSION

As anticipated at section 3.1, the results of petrographic quantitative analysis, i.e. volumetric "modal" analysis, classed all samples of aggregates as potentially alkali-silica reactive due to the presence among their constituents of at least one of those listed as such in the UNI 11530 standard (i.e., chert and chalcedony of carbonate and silicate-bearing rocks (aggregates No. 1, 2, 5, and 6), siliceous microcrystalline matrix of terrigenous rocks (aggregate No. 5), micro-cryptocrystalline quartz of igneous intrusive and silicate-bearing metamorphic rocks (aggregates No. 4, 5 and 6), and, finally, the fine-grained microcrystalline and/or vitreous or glassy groundmass of the volcanic rocks (aggregates No. 3, 5, 6).

Despite the similar reactivity classification of the aggregates, the expansive behaviors in concrete were well differentiated with the occurrence, at the ultimate testing time of UNI 11604 expansion test of results ranging from non-reactive to reactive ones (Figure 9).

Therefore, a first attempt was made to put in relation the recorded expansion results to the contents of potentially alkali-silica reactive constituents of the combined aggregates, derived from the quantitative petrographic analysis, i.e. volumetric "modal" analysis of the grain size fractions, considering the proportions of the various grain size fractions of aggregates in the concrete mixes. For this calculation, the proportions given in Table 2 were used, having verified that there are no appreciable differences between the proportion in weight or volume.

Figure 10 shows the average 365-day expansions of concrete prisms ($\varepsilon_{365\ av}$%) prepared with the aggregates coming from the various sources as a function of the total content of potentially alkali-silica reactive constituents of the aggregate combinations. In the same figure, a line representing the concrete expansion limit of 0.04% for the reactivity of the aggregates is also drawn.

It is well evidenced by Figure 10 that it is not possible to foresee a consistent relationship between the two parameters. So, no value for the total content of the potentially alkali-silica reactive constituents was identified as a critical limit for the reactivity in concrete of the tested aggregates. This suggested the possibility that not all the constituents identified as potentially reactive

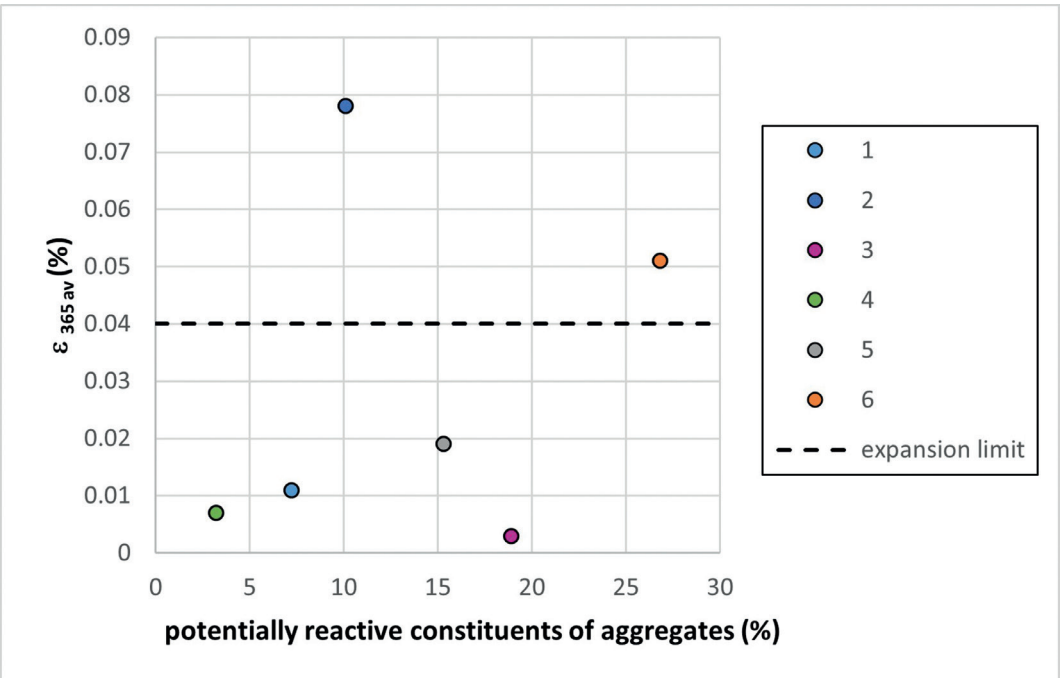

Figure 10. Relationship between average concrete expansions at 365 days of testing and content of potentially ASR constituents of combined aggregates.

by petrographic analysis are such, or that the reactivity of each of them is not equivalent in terms of expansive effects on concrete.

Therefore, further attempts have been made to separately correlate the effects of the various constituents and their contents on the concrete expansion. It was observed that chert and chalcedony were the potentially alkali-silica reactive constituents common to both aggregates responsible for deleterious expansion, i.e., those coming from sources no. 2 and 6. Furthermore, the 365-day expansions of concrete prisms were increasing with the sum of chert and chalcedony contents.

Other than chert and chalcedony of carbonate rocks, micro-cryptocrystalline quartz of igneous intrusive and metamorphic rocks, and microcrystalline groundmass of volcanic rocks were also quantified in aggregates no. 6. Micro-cryptocrystalline quartz was also found in aggregates coming from source no. 1, 4, and 5. Microcrystalline and/or glassy groundmass of volcanic rocks was also found in aggregates no. 3, and to a lesser extent in aggregate no. 5.

As far as the effects of micro-cryptocrystalline quartz contents is concerned, it may be observed that aggregates no. 1, including a 5.4 vol% of this constituent, along with 1.8 vol% of chert + chalcedony, did not cause deleterious expansion in standard concrete prisms. Conversely, aggregates no. 6, characterized by a content of micro-cryptocrystalline quartz of 5.5 vol%, but a higher content of chert + chalcedony (7.1 vol%), caused deleterious expansion in concrete. Moreover, no deleterious expansion was observed using aggregates no. 4, characterized by a 3.2 vol% of micro-cryptocrystalline quartz and free of chert and chalcedony.

As regards the contents of microcrystalline and/or glassy groundmass of volcanic rocks, aggregates no. 3 and no. 5 were very different (18.8 vol% for aggregates no. 3, and 0.7 vol% for aggregates no. 5), but no deleterious expansion in concrete was observed, despite the presence of chert (2.9 vol%) in aggregates no. 5.

The above results suggested a negligible contribution of micro-crystalline quartz and microcrystalline and/or glassy groundmass of volcanic rocks to expansive behavior of aggregates in concrete, and the existence of a relationship between the expansion and the total contents of chert and chalcedony.

As shown in Figure 11 a linear relationship was obtained by plotting the average 365-day expansions of concrete prisms against the sum of chert and chalcedony contents in the concrete aggregates. A critical content value of about 5.5 vol% of chert and chalcedony was found, corresponding to the abscissa of the interception point between the regression line and the horizontal line indicating the expansion limit of 0.04%. It follows that deleterious expansion in concrete will occur for aggregates with a sum of chert and chalcedony contents exceeding the above-mentioned critical value. The same relationship would also lead to the conclusion that the alkali-carbonate reaction, attributable to the presence of

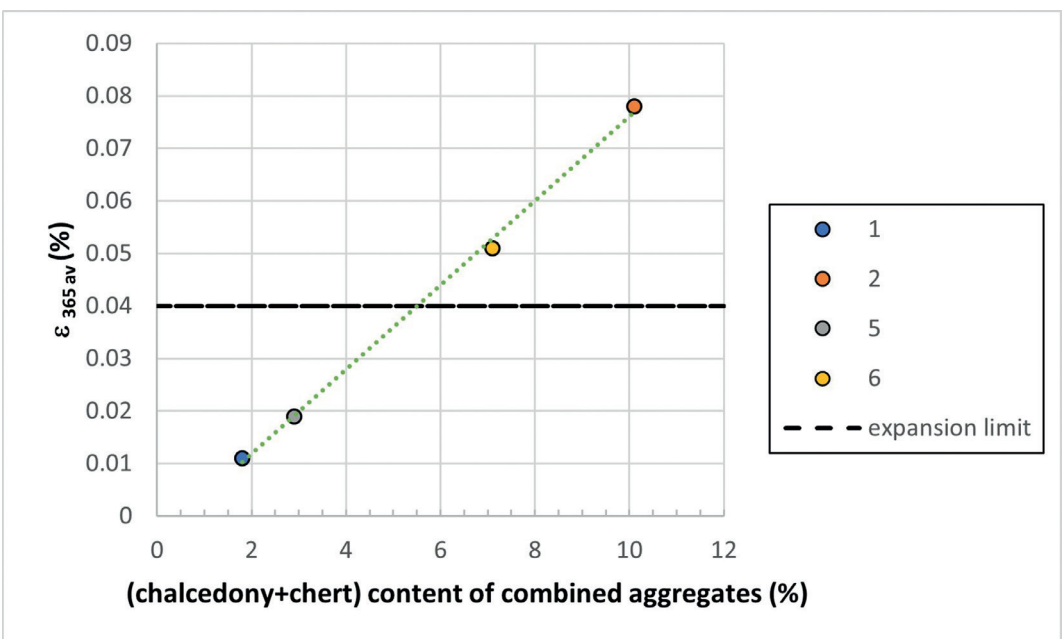

Figure 11. Relationship between average concrete expansions at 365 days of testing and content of (chalcedony + chert) of the combined aggregates.

dolomite, may have not contributed to the expansion in concrete of aggregate 6.

CONCLUSIONS

The practical implications of the study of the correlation between the petrographic quantitative analysis and concrete expansion test results shown in this paper are:

1. The petrographic analysis of the aggregates highlighted the widespread presence of constituents defined as potentially alkali-silica reactive by the standard UNI 11530, but the extent of the concrete prism expansion was found to depend on the type of constituent. The correlation analysis showed that lithotypes that contribute most to expansion are chert and chalcedony, while micro-crystalline quartz or microcrystalline and/or glassy groundmass of volcanic rocks produce limited expansive effects.
2. Congruent reactivity evaluations will be expected for aggregates subjected to both concrete expansion test and quantitative petrographic examination coupled with the critical content value of chert and chalcedony of aggregates.
3. The quantitative petrographic examination, or "modal" analysis, coupled with the critical content value could represent a significant and strong tool for predicting the expansive behavior (deleterious or not deleterious) of aggregates in concrete prism test UNI 11604.

However, further investigation on a wide variety of aggregates is required to better define the critical content of potentially alkali-silica reactive constituents.

ACKNOWLEDGEMENTS

The Authors are grate to blind revisors for the constructive critical review of the paper.

REFERENCES

Alunno Rossetti V., 1981. Osservazioni di pop-outs dovuti alla reazione alcali aggregati su pavimentazioni in calcestruzzo in Italia. La Prefabbricazione, giugno 1981.

Antolik A. and Józwiak-Niedzwiedzka D., 2021. Assessment of the alkali-silica reactivity potential in granitic rocks. Construction and Building Materials 295, 123690. doi: 10.1016/j.conbuildmat.2021.123690.

Antolik A., Dąbrowski M., Jóźwiak-Niedźwiedzka D., 2023. Petrographic Evaluation of Aggregate from Igneous Rocks: Alkali-Silica Reaction Potential. Minerals 13, 1004. doi: 10.3390/min13081004.

Bavasso I., Costa U., Mangialardi T., Paolini A.E., 2020. Assessment of Alkali–Silica Reactivity of Aggregates by Concrete Expansion Tests in Alkaline Solutions at 38 °C. Materials 13, 288. doi: 10.3390/ma13020288.

Barisone G., 2001. Microscopical determination of flint content in the alluvial deposits of Italian Peninsula. Proc. 8th Euroseminar on Microscopy Applied To Building Materials (EMABM 2001), Athens (Greece), 1-6.

Berra M., Mangialardi T., Paolini A.E., 2005. Alkali-silica reactivity criteria for concrete aggregates. Materials and Structures 38, 373-380. doi: 10.1007/BF02479304.

Berra M., Costa U., Mangialardi T., Paolini A.E., 2015. Application of an innovative methodology to assessing the alkali-silica reaction in concrete. Materials and Structures 48, 2727-2740. doi: 10.1617/s11527-014-0349-9.

Beyene M.A., Snyder A., Lee R.J., Blaszkiewicz, 2013. Alkali Silica Reaction (ASR) as a root cause of distress in a concrete made from Alkali Carbonate Reaction (ACR) potentially susceptible aggregates. Cement and Concrete Research 51, 85-95. doi: 10.1016/j.cemconres.2013.04.014.

Beyene M.A. and Meininger R.C., 2018. Alkali Reactive Carbonate Rocks: Is it Alkali Silica Reaction (ASR) or Alkali Carbonate Reaction (ACR)? Proc. 6th International Conference on Durability of Concrete Structures, Leeds (UK), 281-289.

Bish D. and Howard S., 1988. Quantitative phase analysis using the Rietveld method. Journal of Applied Crystallography 21, 86-91. doi: 10.1107/S0021889887009415.

Bon E., Chille F., Masarati P., Massaro C., 2001. Analysis of the Effects Induced by Alkali-Aggregate Reaction (AAR) on the Structural Behavior of Pian Telessio Dam. Proc. 6th International Benchmark Workshop on Numerical Analysis of Dams (Theme A), Salzburg (Austria).

Borchers I., Lindgård J., Rønning T.F., Wigum B.J., 2021. Recommendation of RILEM TC 258-AAA: RILEM AAR-11: determination of binder combinations for non-reactive mix design or the resistance to alkali-silica reaction of concrete mixes using concrete prisms - 60 °C test method. Materials and Structures, 54, 203. doi: 10.1617/s11527-021-01680-3.

Borchers I., Lindgård J., Müller C., 2022. Evaluation of laboratory test methods for assessing the alkali-reactivity potential of aggregates by field site tests. Materiales De Construcción 72, 346, e286. doi: 10.3989/mc.2022.17221.

Costa U., Mangialardi T., Paolini A.E., 2014. Assessment of blended cements effectiveness against ASR by mortar and concrete expansion tests. Journal of Advanced Concrete Technology 12, 266-278. doi: 10.3151/jact.12.266.

Costa U., Mangialardi T., Paolini A.E., 2017. Minimizing alkali leaching in the concrete prism expansion test at 38 °C. Construction and Building Materials 146, 547-554.

Custódio J., Costa D., Bettencourt Ribeiro A., Santos Silva A., 2022. Assessment of potential alkali-silica reactivity of aggregates for concrete. Procedia Structural Integrity 37, 590-597.

Doğruyol M., 2024. Determination of ASR in Concrete Using Characterization Methods. Buildings 2024, 14, 657. doi: 10.3390/buildings14030657.

Dunham R., 1962. Classification of carbonate rocks according

to depositional texture. American Association of Petroleum Geologists Mem. 1, 108-121.

Embry A. and Klovan J., 1971. A Late Devonian reef tract on Northeastern Banks Island. Bulletin of Canadian Petroleum Geology 19, 730-781.

Fernandes I., Broekmans M., dos Anjos Ribeiro M., Martins H., Sims I., 2014. Petrographic identification of alkali-reactive aggregates, including siliceous carbonates. Proc. 14th International Multidisciplinary Scientific GeoConference & EXPO (SGEM), Albena (Bulgaria), 715-722.

Fernandes I., Broekmans M., dos Anjos Ribeiro M., Sims I., 2020. Assessment of the alkali-reactivity potential of sedimentary rocks. Proc. 15th International Conference on Alkali-Aggregate Reaction (ICAAR 2019), Sao Paulo (Brazil).

Fettes D. and Desmons J., 2007. Metamorphic Rocks: A Classification and Glossary of Terms: Recommendations of the International Union of Geological Sciences Subcommission on the Systematics of Metamorphic Rocks. Cambridge, University Press, Cambridge (UK).

Flügel E., 2010. Microfacies of Carbonate Rocks. Analysis, interpretation and application. Springer-Verlag, Berlin Heidelberg (Germany), doi: 10.1007/10.1007/978-3-642-03796-2.

Folk R., 1980. Petrology of Sedimentary Rocks. Hemphill Publishing, Austin (USA).

Friedman G., 1959. Identification of carbonate minerals by staining methods. Journal of Sedimentary Petrology 29, 87-97.

Garzanti E., 2019. Petrographic classification of sand and sandstone. Earth-Science Reviews 192, 545-563. doi: 10.1016/j.earscirev.2018.12.014.

Gasparotto G., Bargossi G.M., Peddis F., Sammassimo V., 2011. A case study of alkali-silica reactions: petrographic investigation of paving deterioration. Periodico di Mineralogia 80, 309-316. doi: 10.2451/2011PM0022.

Giuseppetti G., Donghi G., Marcello A. (Eds.), 2003. Experimental investigations and numerical modelling for the analysis of AAR process related to Poglia dam: evolutive scenarios and design solution. In: Dam Maintenance and Rehabilitation, Routledge (1st edition), London (UK).

Jensen V., 2012. The controversy of alkali carbonate reaction: state of art on the reaction mechanisms and behaviour in concrete. Proc. 14th International Conference on Alkali-Aggregate Reaction (ICAAR 2012), Austin (USA).

Jensen V., 2020. Diagnosis of alkali silica reaction. Proc. 15th International Conference on Alkali-Aggregate Reaction (ICAAR 2019), Sao Paulo (Brazil). https://icaarconcrete.org/wp-content/uploads/2020/11/15ICAAR-JensenV-2.pdf.

Le Maitre R.W. (Ed.), 2005. Igneous Rocks: A Classification and Glossary of Terms: Recommendations of the International Union of Geological Sciences Subcommission on the Systematics of Igneous Rocks, Cambridge University Press (2nd edition), Cambridge (UK).

Levi F., Mancini G., Napoli P., 1985. Structural damages due to the alkali silica reaction (ASR). L'Industria Italiana delle Costruzioni 169, 59-73.

Marinoni N., Voltolini M., Mancini L., Cella F., 2012. Influence of aggregate mineralogy on alkali-silica reaction studied by X-ray powder diffraction and imaging techniques. Journal of Materials Science 47, 2845-2855. doi: 10.1007/s10853-011-6114-3.

Marinoni N. and Broekmans M., 2013. Microstructure of selected aggregate quartz by XRD, and a critical review of the crystallinity index. Cement and Concrete Research 54, 215-225. doi: 10.1016/j.cemconres.2013.08.007.

Medeiros S., Fernandes I., Fournier B., Nunes J., Santos-Silva A., Ramos V., Soares D., 2022. Alkali-silica reaction in volcanic rocks: a worldwide comparative approach. Materiales De Construcción 72, 346, e278. doi: 10.3989/mc.2022.16221.

Rigaku, 2015. Quantitative analysis of dolomite and limestone by pressed powder method with Supermini 200. Rigaku Application note XRF 1058. https://www.rigaku.com/applications/wdxrf1058.

Rønning T.F., Wigum B.J., Lindgård J., Nixon P., Sims I., 2021. Recommendation of RILEM TC 258-AAA: RILEM AAR-0 outline guide to the use of RILEM methods in the assessment of the alkali-reactivity potential of concrete. Materials and Structures 54, 206. doi: 10.1617/s11527-021-01687-w.

Rønning T.F., Wigum B.J., Lindgård J., 2021. Recommendation of RILEM TC 258-AAA: RILEM AAR-10: determination of binder combinations for non-reactive mix design using concrete prisms - 38 °C test method. Materials and Structures 54, 204. doi: 10.1617/s11527-021-01679-w.

Saouma V. and Perotti L., 2005. Alkali Aggregate Reaction in Dams, Stress Analysis and Long Term Predictions. Proc. ASDSO, Dam Safety Conference, New Orleans (USA), 19 p.

Sibley D.F. and Gregg J.M., 1987. Classification of Dolomite Rock Textures. Journal of Sedimentary Research 57, 967-975.

Sims I. and Poole A., 2017. Alkali-Aggregate Reaction in Concrete: A World Review. CRC Press, Taylor & Francis Group, London (UK).

Streckeisen A., Zanettin B., Le Bas M. J., Bonin B., Bateman P., 2002. Igneous Rocks: A Classification and Glossary of Terms. Recommendations of the International Union of Geological Sciences Subcommission on the Systematics of Igneous Rocks. R.W. Le Maitre & International Union of Geological Sciences 2002. doi: 10.1017/CBO9780511535581.

Tritsch S.L., 2018. Alkali Carbonate Reaction An Ongoing Study. Proc. 51st Annual Mid-Atlantic Quality Assurance Workshop, February 13-15th, 2018, Dover, Delaware (USA), 1-22.

Tucker M. and Wright W., 1990. Carbonate Sedimentology, Blackwell Science Publishing, Oxford (UK).

UNI EN 197-1, 2011. Cemento - Parte 1: Composizione, specificazioni e criteri di conformità per cementi comuni.

UNI EN 933-1, 2012. Prove per determinare le caratteristiche geometriche degli aggregati: Determinazione della distribuzione granulometrica - Analisi granulometrica per setacciatura.

UNI EN 1097-6, 2022. Prove per determinare le proprietà meccaniche e fisiche degli aggregati - Parte 6: Determinazione della massa volumica dei granuli e dell'assorbimento d'acqua.

UNI EN 12620, 2008. Aggregati per calcestruzzo. UNI - Ente Italiano di Normazione.

UNI 8520-22, 2020. Aggregati per calcestruzzo - Parte 22: Metodologia di valutazione della potenziale reattività alcali-silice degli aggregati. UNI - Ente Italiano di Normazione.

UNI 11417-2, 2022. Durabilità delle opere di calcestruzzo e degli elementi prefabbricati di calcestruzzo - Parte 2: Indicazioni per prevenire la reazione alcali-silice. UNI - Ente Italiano di Normazine.

UNI 11504, 2021. Reazione alcali-aggregato in calcestruzzo - Determinazione della potenziale reattività agli alcali degli aggregati per calcestruzzo - Prova di espansione accelerata di barre di malta. UNI - Ente Italiano di normazione.

UNI 11530, 2023. Reazione alcali-aggregato in calcestruzzo - Determinazione della potenziale reattività agli alcali degli aggregati per calcestruzzo - Esame petrografico di dettaglio dell'aggregato per la determinazione dei costituenti potenzialmente reattivi. UNI - Ente Italiano di normazione.

UNI 11604, 2020. Reazioni alcali-aggregato in calcestruzzo - Determinazione della potenziale reattività agli alcali degli aggregati per calcestruzzo - Prova di espansione accelerata in calcestruzzo. UNI - Ente Italiano di normazione.

Vola G., Berra M., Rondena E., 2011. Petrographic quantitative analysis of ASR susceptible Italian aggregates for concrete. Proc. 13th Euroseminar on Microscopy Applied to Building Materials (EMABM 2011), Ljubljana (Slovenia), 9 p.

Young R. (Ed.), 1993. The Rietveld Method, IUCr Monograph on Crystallography, Oxford University press, Oxford (UK).